ACS Catalysis

RESEARCH ARTICLE

pubs.acs.org/acscatalysis

Field Effects in Plasmonic Photocatalyst by Precise SiO_2 Thickness Control Using Atomic Layer Deposition

Manippady Krishna Kumar,* Sivashankar Krishnamoorthy, Lee Kheng Tan, Sing Yang Chiam, Sudhiranjan Tripathy, and Han Gao

Institute of Materials Research and Engineering, A*STAR (Agency for Science, Technology and Research), 3 Research Link, Singapore 117602

Supporting Information

ABSTRACT: We report on TiO_2 thin films with superior photocatalytic efficiency due to an increase in its exciton carrier generation induced by the plasmonic field of the underlying silver nanoparticles. TiO_2 thin films are deposited on supported silver nanoparticles and are separated from each other by a fine-tunable thickness of SiO_2 interlayer. The TiO_2(15 nm)/SiO_2/Ag nanoparticle architectures with systematic variation of SiO_2 interlayer thickness of 2, 5, 10, and 20 nm show systematic increase in photocatalytic efficiency with decrease in the SiO_2 thickness. The efficiency enhancement is shown to be caused by plasmonically enhanced carrier generation, which was confirmed through photocurrent measurements and Raman spectroscopy. With a 2 nm SiO_2 interlayer that exhibited the best photocatalytic performance, a 3 times increase in photocurrent density, and a 200 times increase in Raman signal intensity of TiO_2 is found. Atomic layer deposition was employed to achieve precise film thickness control of SiO_2 and TiO_2 layers.

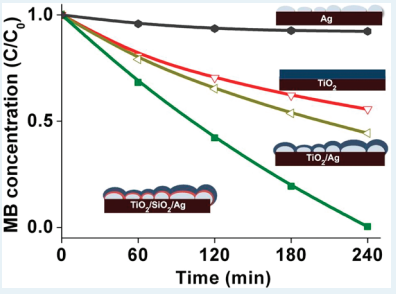

KEYWORDS: plasmonic photocatalysis, atomic layer deposition (ALD), titanium dioxide

INTRODUCTION

An efficient supported photocatalyst for air and water remediation is highly sought after. Ideally, such photocatalyst needs to exhibit efficient absorption of photons across the UV−visible region of the solar spectrum, high photon to electron hole (e^-/h^+) pair conversion efficiency, low e^-/h^+ pair recombination rates, and low activation barrier toward the surface redox half reactions.[1,2] In this regard, titanium dioxide (TiO_2) based catalysts in different forms have been extensively investigated,[3,4] because of their high photocatalytic efficiency combined with advantages of chemical stability, nontoxicity, and low-cost.[1,3,5] However, with a typical TiO_2 band gap of 3.2 eV (388 nm), only ∼4% of the solar spectrum can be utilized. Additionally, TiO_2 suffers from considerable recombination of the photogenerated e^-/h^+ pairs. Countering these challenges are very important for the widespread application of TiO_2 as a photocatalyst. Several approaches in this direction have been pursued, namely, TiO_2-composites with quantum dots such as CdS, CdSe, InP, or PbS and doping of TiO_2 with nonmetals are used to tune or engineer the bandgap, use of TiO_2 nanostructures such as tubes, rods or particles are also explored to lower e^-/h^+ recombination while finally, composites of TiO_2 with metals is also an actively pursued research.[1−5] The use of metals is commonly employed to inhibit e^-/h^+ pair recombination with the metal particles acting as irreversible electron sinks.[6] The metals having a Fermi level that is lower than that of TiO_2 can collect the photoexcited electrons from the conduction band of TiO_2 thus helping in efficient charge separation resulting in a higher photocatalytic reaction rate. Among these metals, Ag is a popular choice because of its high work function and its ability to generate surface plasmons at the desired wavelength.[7,8] Ag can be integrated either by coating of TiO_2 surface with Ag particles or in a composite form with TiO_2. Both of these architectures suffer from certain disadvantages: a high concentration of Ag particles can lead to UV shielding as well as a reduction of reactive surface sites available for catalysis.[9,4] In the later case, silver could even reduce the crystallinity of TiO_2. It is therefore advantageous to have an architecture whereby the Ag nanoparticles/film are placed beneath the TiO_2 film. However, in this approach, there is a trade-off between the thickness of the TiO_2 film and the beneficial influence of the Ag. This is because a photocatalytically efficient thick TiO_2 film could be opaque, the Ag nanoparticles film at the bottom of such a thick film would not bring out its efficacy. For this reason, we study the use of ultrathin TiO_2 films that are only 15 nm thick over supported Ag nanoparticles to maximize Ag induced enhancement in photocatalytic efficiency. This architecture removes constraints on the maximum concentration of Ag nanoparticles that can be used. We demonstrate this by using a highly thickness controlled and conformally coated TiO_2 on top of Ag nanoparticles on Si surface. We particularly focus on the enhancement of the photocatalytic efficiency by Ag induced plasmonic field effects rather than by Ag as electron sink. This is

Received: December 2, 2010
Revised: January 26, 2011
Published: February 28, 2011

shown by introducing a thin and conformal SiO_2 interlayer that separates TiO_2 and Ag.

Such plasmonic enhanced photocatalysis was first proposed by Awazu et al. in a structure consisting of TiO_2 over SiO_2 covered Ag nanoparticles.[10] The surface plasmon is due to the photo-induced collective oscillation of conduction electrons (i.e., localized surface plasmon resonance, LSPR).[7] The large close vicinity electric field enhancement (i.e., near field effect), so generated because of Ag nanoparticles, and the LSPR mediated far field scattering (i.e., far field effect) due to radiative decay of surface plasmon lead to a prolonged optical path which can beneficially boost the excitation of e^-/h^+ pairs in TiO_2.[10] The SiO_2 with a refractive index (at 400 nm) of 1.54 is used as an interlayer since it does not restrict in the creation and coupling of the LSPR energy from Ag nanoparticles to TiO_2.[10] We add that Ag nanoparticles are also an ideal metal to investigate near-field coupling since the plasmon resonance of Ag nanoparticles lies close to the electronic energy band gap of TiO_2.[10] In this architecture of plasmonic enhanced photocatalysis, the control and engineering of TiO_2-SiO_2-Ag nanoparticles interfaces and the respective film thickness are vital. Through the use of atomic layer deposition (ALD), we can achieve controllable and conformal coating of both the SiO_2 and the TiO_2 thin films that are not achievable through other coating approaches such as sputtering, thermal evaporation or sol−gel process. Through this precise control over both the density of Ag nanoparticles and the distance between Ag and TiO_2 layers (through the SiO_2 interlayer), we can clearly investigate the role of Ag and its accompanying mechanisms that are responsible for the enhancement in photocatalysis.[11]

EXPERIMENTAL SECTION

Experimental Procedures. *Silver Nanostructures Preparation.* The silver nanoparticles on Si substrate were prepared by the galvanic displacement (GD) process on a silicon substrate in an ionic metal HF solution.[12] A square silicon substrate of area 5 cm^2 were degreased by sonication in acetone and isopropanol for 10 min and then rinsed with deionized water (22 MΩ) before drying in gentle N_2. A native oxide layer was etched out by immersing the chips in a diluted (1%) aqueous HF solution for 3 min followed by rinsing in DI water and subsequent drying with N_2. Silver plating solution contained 0.02 mol L^{-1} of $AgNO_3$ and 1% HF in DI water. Silicon chips were immersed right after native oxide etching and left in solution for the desired time at room temperature. DI rinsing and N_2 drying were performed after deposition.

ALD of TiO_2 and SiO_2. TiO_2 and SiO_2 thin films were deposited in an f·XALD ALD equipment (Azimuth Technologies Pte Ltd., Singapore). The procedure for ALD has been described elsewhere.[13,14] Briefly, $TiCl_4$ (Merck, 99%) and H_2O (deionized water), were sequentially introduced into a viscous flow ALD chamber in pulses at 150 °C. The respective durations for exposure and purge for the precursors are 0.01 s $TiCl_4$ - 10 s N_2 purge- 0.01 s H_2O - 10 s N_2 purge. Similarly, SiO_2 ALD too was performed at room temperature by the sequential $SiCl_4$ (Sigma-Aldrich, 99.998%) and H_2O along with co-dose of anhydrous pyridine (Sigma-Aldrich, C_5H_5N, 99.8%).[14] The film thickness was easily controlled by counting the number of respective ALD cycles. The ALD growth rate was confirmed by a variable angle spectroscopic ellipsometer (J.A. Woolam Company). Anatase crystalline TiO_2 was obtained after annealing the as-prepared TiO_2 in air at 500 °C for 2 h.

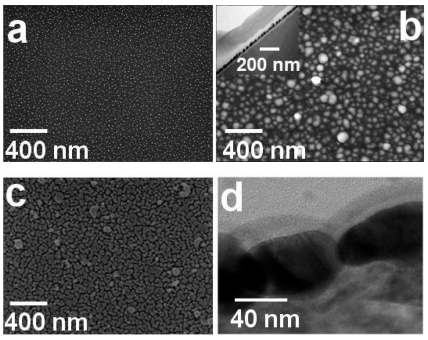

Figure 1. SEM images of Ag nanoparticles on Si substrates obtained by the GD technique with a growth duration of (a) 1 min (Sample 1) showing Ag nanoparticles of size ∼10−20 nm with well separated spacing of 20−50 nm; (b) 2 min (Sample 2) showing Ag nanoparticles of size ∼60−150 nm with a typical spacing of M< 15 nm. The inset shows a cross sectional TEM image of the sample; (c) 5 min (Sample 3) showing highly textured Ag film that exhibits a mirror like surface visually; (d) TEM micrograph showing a cross section view of 15 nm TiO_2/2 nm SiO_2/sample 2 after annealing in air at 500 °C for 2 h. The uniform, compact, and ultrathin TiO_2 film is coated on Ag nanoparticles, with a 2 nm SiO_2 interlayer. Clear and distinct interface between the Ag-SiO_2 and SiO_2-TiO_2 are achievable by ALD, and the quality of these interfaces are shown to be intact even after the annealing.

Characterization of the Samples. *Photocatalysis.* The sample with a surface area of 5 cm^2,was immersed in 5 mL of unstirred MB ($C_{16}H_{18}-ClN3S\cdot xH_2O$, Sigma-Aldrich) with an initial dye concentration of $Co = 1.0 \times 10^{-5}$ M. This was exposed to long wavelength UV light (Brand: Vilber Lourmat France, model: Biolink), with a maximum at 365 nm. The films were placed at a distance of 10 cm from the lamp, and the corresponding irradiation intensity was 17 $\mu W/cm^2$. The photodegraded MB Solution was analyzed using a UV−vis−NIR scanning spectrophotometer (Shimadzu UV 3101) after every 1 h of UV exposure. For comparison, the MB solution was also photolyzed in the absence of photocatalyst, in the dark and also with Ag nanoparticles only.

Photocurrent Measurements. The photocurrent density in the TiO_2 film upon an illumination over an area of ∼3 cm^2 was measured using EG&G model 273 potentiostat/galvanostat in a three electrode cell with Pt mesh cathode counter electrode and Ag/AgCl reference Electrode in 0.1 M KCl solution under UV illumination (Hamamatsu UV spot light source LC5, maximum 365 nm ∼1.25 mW/cm^2).[15,16] The photo anode was anodically polarized to 0.5 V under illumination, and the photocurrent was recorded.

SEM, XPS, TEM, Raman, XRD Characterization. Scanning electron microscopy (SEM) was performed using JSM-6700F FESEM (JEOL, Tokyo, Japan). X-ray photoelectron spectroscopy (XPS, VG ESCALab 220i-XL) using a monochromated Al Kα excitation source was carried out to investigate the chemical state of the Ag nanoparticles. High resolution transmission electron microscopy (HRTEM, Philips CM300) operating at 300 kV was used to study the cross section and interface structure of the film. The sample for cross-sectional HRTEM was prepared by bonding the top surfaces of 2 pieces of 3 mm ×1 mm samples with epoxy glue. The sample was cured and subsequently polished using graphite lapping film until about 10−50 μm thick. The sample was dimpled and finally ion milled. Reflectance

dx.doi.org/10.1021/cs100117v |ACS Catal. 2011, 1, 300–308

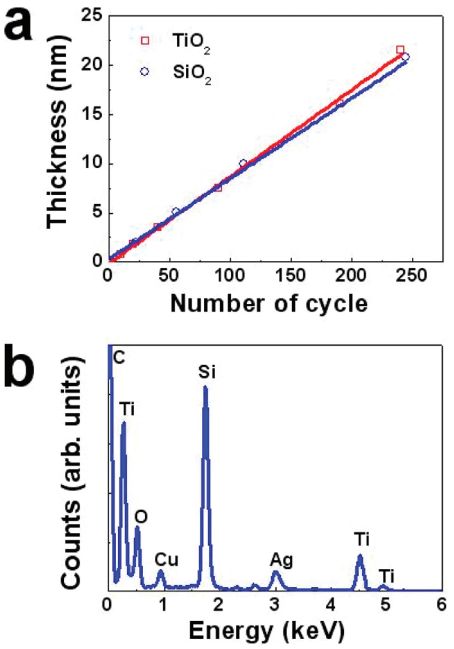

Figure 2. (a) Atomic-layer control of film thickness by ALD: linear relation of the film thickness versus the number of ALD cycles confirms the goodness of the ALD growth process with the following scheme 0.01 s $TiCl_4$ - 10 s N_2 purge- 0.01 s H_2O - 10 s N_2 purge at 150 °C. SiO_2 ALD was performed at 25 °C by a similar sequential with $SiCl_4$ and H_2O along with co-dose of anhydrous C_5H_5N. (b) EDX spectra for TiO_2/SiO_2/sample 2, showing the constituent Ti, Si, and Ag elemental identity of the sample.

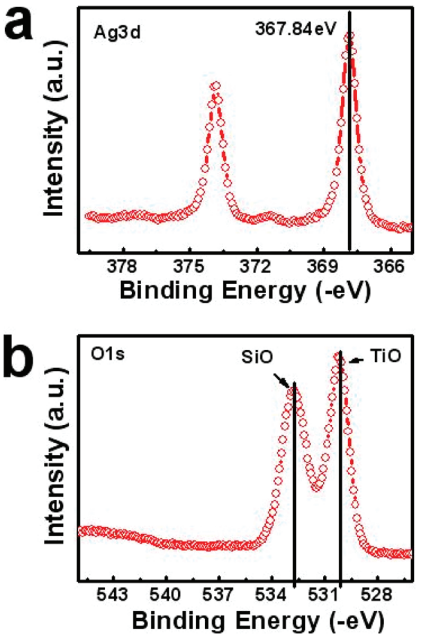

Figure 3. XPS spectrum of annealed 2 nm TiO_2/2 nm SiO_2/sample 2 showing the (a) Ag 3d and (b) Ag O 1s confirms that an immediate coat of a SiO_2 over the Ag nanoparticles preserves Ag in its metallic Ag (0) form.

measurements were carried out in microspectrophotometer from CRAIC (Craic Technologies, CA, U.S.A.). The reflectance spectra are collected against TiO_2/sample 3 film as reference.[17] The spectra of only Ag nanoparticles were recorded with just Ag film as the reference. Raman spectra of all the samples were collected using a micro-Raman system (Jobin-Yvon T64000) with 325 nm UV excitation. X-ray diffraction (XRD) analysis was carried out using Cu Kα radiation in a Siemens D5000 diffractometer provided with a thin film attachment.

RESULTS AND DISCUSSION

Photocatalytic Sample Preparation and Characterization. The Ag nanoparticles on Si substrate were prepared by a GD reaction in a mixture of silver nitrate and HF bath.[18] GD allows for controlled growth of oxide-free Ag nanostructures by a careful selection of both the growth period and the concentration of the silver salt. The representative plain view SEM images of Ag nanostructures obtained for growth periods of 1, 2, and 5 min are shown in Figure 1a−c. Henceforth, these samples will be identified as sample 1, 2, and 3, respectively. In sample 1, the Ag nanoparticles of sizes 10−20 nm are observed to be well separated by typical spacing in the range of 20−50 nm (Figure 1a). In sample 2, the particle sizes are ∼60−150 nm (Figure 1b) with interparticle spacings of <15 nm. The inset in Figure 1b shows an HRTEM image of sample 2. Sample 3, grown for 5 min as shown in Figure 1c, results in a thick Ag film with a textured surface. This is visually mirror like and is used as a reference for our optical characterizations.[17]

Generally, the LSPR decays either radiatively by the resonant scattering process and/or via a nonradiative absorption caused by electron−phonon interactions.[19] It has been reported that the radiative decay usually dominates for spherical particles larger than about 40 nm.[7] Moreover, it has also been demonstrated that localized electric field intensity can be significantly increased with the decrease in the spacing between nanoparticles.[20] It is also known that the e-field enhancement due to coupling between adjacent nanoparticles also increase exponentially as a function of separation.[7,19] If we consider utilizing the strong plasmon near-field effect, larger silver nanoparticles that exhibit a smaller interparticle separation would be particularly suitable. These requirements are better met in sample 2, than in sample 1. Therefore sample 2 will be a more suitable candidate to not only achieve better photocatalytic efficiency but also understand the mechanism in enhancement.

In the next step, the Ag nanoparticles in samples 1−3 were coated with 2, 5, 10, and 20 nm of SiO_2 followed by a 15 nm TiO_2 film using ALD. The SiO_2 film serves two purposes. First as a protective interlayer to prevent Ag from oxidization, and more importantly, to effectively tune the LSPR of Ag to match the absorption edge of TiO_2. SiO_2 is also attractive because of its inertness and optical transparency in the UV−vis−near IR wavelength range that are of interest. It is useful in this context to point out that oxides such as SiO_2 or Al_2O_3 have been used as an ultrathin spacer layer in Surface Enhanced Raman Scattering (SERS) experiments with the aim to protect the SERS active metallic nanoparticles.[21,22]

The role of ALD in forming a well-defined and high-integrity TiO_2−SiO_2−Ag multilayer architecture needs to be emphasized. ALD is a very useful technique in this respect as it can provide digital-like film thickness control by simply varying the number of ALD cycles. Figure 2a shows the plot of both the SiO_2 and the TiO_2 film thickness versus the number of ALD cycles obtained using our ALD parameters. The growth rate can be observed to be linear, indicating the well controlled nature of the ALD process. The ALD of SiO_2 on Ag nanoparticles is made

dx.doi.org/10.1021/cs100117v |ACS Catal. 2011, 1, 300–308

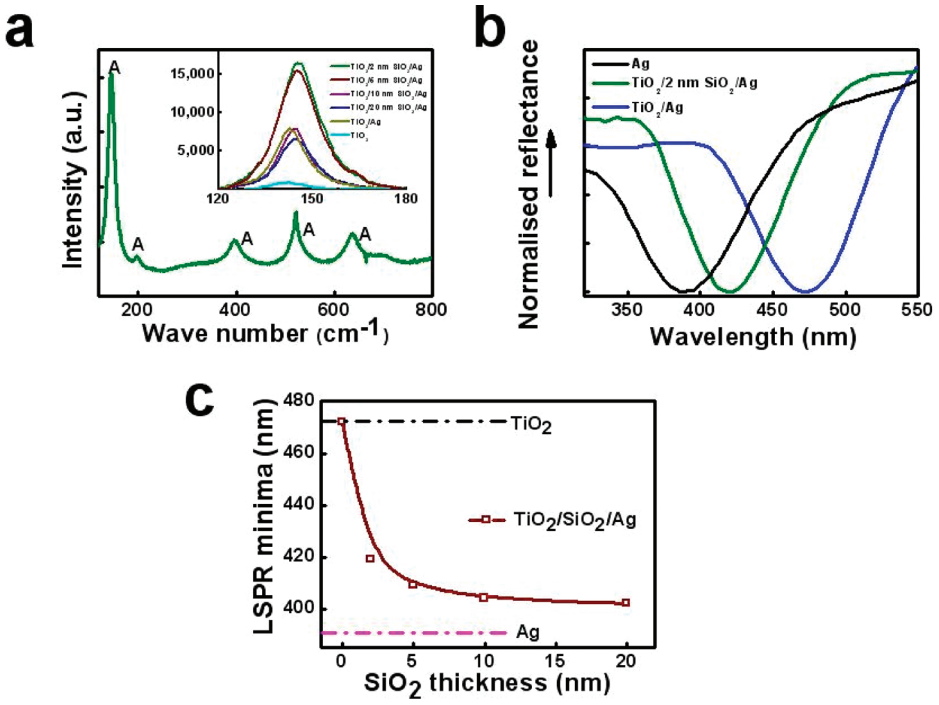

Figure 4. (a) Raman spectra for TiO_2 in TiO_2/2 nm SiO_2/Sample 2 showing the bands at 144 cm^{-1}, 197 cm^{-1}, 396 cm^{-1}, 514 cm^{-1}, and 635 cm^{-1}; consistent with the anatase phase. The inset is the normalized Raman peak corresponding to 144 cm^{-1} showing the SiO_2 interlayer thickness dependent SERS response. (b) Normalized UV−vis reflectance spectra of TiO_2/Sample 2, TiO_2/2 nm SiO_2/Sample 2, and Sample 2. The LSPR identified by the reflectance minima undergoes a red shift upon Ag nanoparticles coating with TiO_2 and TiO_2/SiO_2. (c) LSPR wavelength vs SiO_2 film thickness showing the subdued red shift upon increase of the SiO_2 interlayer thickness.

possible because of very thin innate oxide layer over the Ag nanoparticles.[23] Each cycle for ALD of SiO_2 consisted of alternating exposure to $SiCl_4$ and H_2O along with a co-dose of pyridine. Because of its basicity, pyridine renders oxygen of the surface hydroxyl groups a stronger nucleophile by forming strong hydrogen bonds with the H-atoms.[14] Therefore, this chemistry allows for the low temperature ALD of SiO_2. Further, the room temperature ALD of SiO_2 ensures that the Ag nanoparticles do not get sintered and oxidized.[24] The low temperature sintering, which is much below the melting point of silver (960 °C), is attributed to the reduced melting point of nanoparticles compared with that of bulk metal and to the surface premelting.[24] It is important to note that the use of pyridine does not result in the incorporation of N or C into the deposited SiO_2 film.[14] We have also confirmed this finding from the XPS analysis of the ALD of SiO_2 films. The ALD of TiO_2 was performed using $TiCl_4$ and H_2O as precursors at a temperature of 150 °C. Cross-sectional TEM analysis (Figure 1d) clearly confirms the thickness and conformality of both the SiO_2 and the TiO_2 films for all samples used. The Ag nanoparticles are observed to anchor well onto the Si substrate. The EDX spectrum (Figure 2b) also correctly shows the elemental composition of the TiO_2, SiO_2, and Ag structure. Figure 3 shows the XPS spectra for the annealed 2 nm TiO_2/2 nm SiO_2/Ag nanoparticles film surface composition. Since our interest in carrying out the XPS analysis is to confirm the ability of the inert SiO_2 interlayer in preserving the Ag nanoparticles in their metallic form for the completely processed sample, in this study we have provided the XPS analysis only for the annealed samples. The Ag 3d spectrum of Ag-TiO_2 as shown in Figure 3a consists of two peaks at 367.84 and 374.3 eV for Ag $3d_{5/2}$ and Ag $3d_{3/2}$, respectively. This corresponds well with the metallic Ag(0) state.[25] However, we note that this measured peak is slightly less than the value of 368.2 eV we routinely obtain for the Ag $3d_{5/2}$ for a polycrystalline Ag foil. This is not a case of oxidized Ag as the O1s peak measured did not show any AgO (528.6 eV) or Ag_2O (529.5 eV) peaks.[26] Instead, a binding energy of 530.32 eV and 532.82 eV is observed for the O1s peak as shown in Figure 3b. While we did not include the contribution from chemisorbed C−O in the peak fit that can be present, it is clear that no oxidized silver can be observed from the O1s. The significant shift between these two peaks is caused because of the differential charging in the two oxide materials.[27,28] Furthermore, oxidized Ag3d will have typically a larger fwhm in a line shape analysis.[29] Our measured fwhm of 0.74 eV is in good agreement with that of polycrystalline Ag foil (0.71 eV) considering that a slightly larger fwhm is expected with the TiO_2 overlayer. More importantly, weak surface plasmon satellites loss can be observed at higher binding energies as seen in Figure 3a that shows conclusively that the measured Ag has metallic properties. There can be several reasons behind the smaller binding energy of Ag3d as compared with a typical Ag foil measurement, such as particle size effect, Ag−Si interactions, extra-atomic relaxation effects, defects interaction, or even strain effects.[30] In this instance, we attribute the lower binding energy of the Ag3d to the additional screening provided by the close proximity of the Si substrate (extra-atomic relaxation effects).[30] We can therefore be confident in concluding that the immediate coating of a very thin layer of SiO_2 over the Ag nanoparticles largely preserves Ag in its metallic form, and this passivation is intact even after a high temperature anneal. To confirm the absence of Ag migration, we have performed XPS for a sample with a thicker SiO_2 interlayer. The sample architecture is 15 nm TiO_2/2 nm SiO_2/Sample 2. As expected, for this sample we do not observe any signature spectra due to Ag.

dx.doi.org/10.1021/cs100117v |ACS Catal. 2011, 1, 300–308

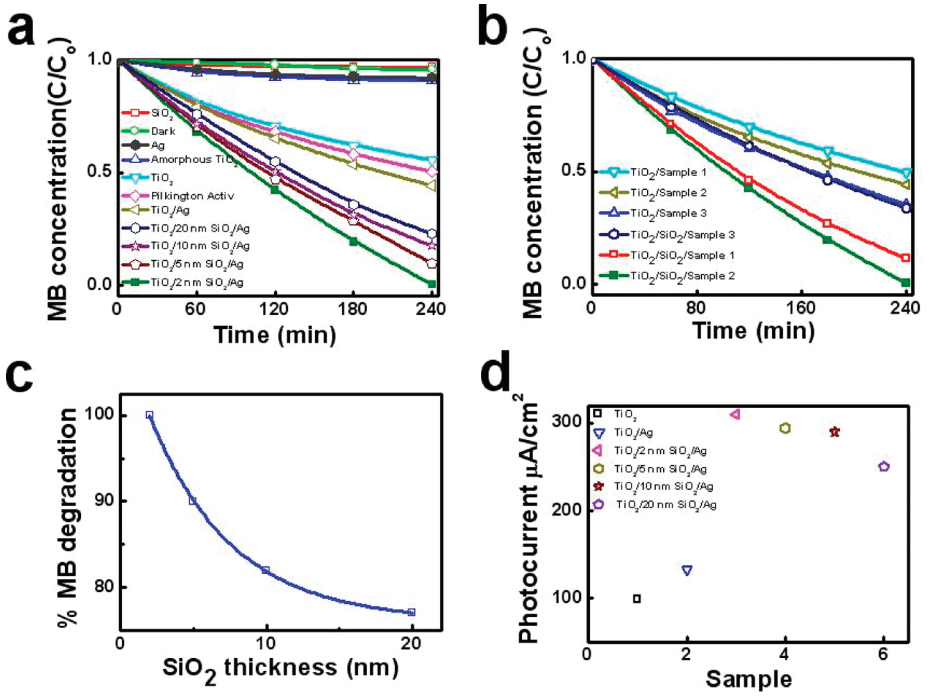

Figure 5. Kinetic data of photocatalytic mineralization of methylene blue (MB) in the presence of (a) pure TiO_2; TiO_2 film coated over sample 2; TiO_2 over sample 2 with SiO_2 interlayer of thickness 2, 5, 10, and 20 nm. The kinetic is characterized by monitoring the degradation of 5 mL MB of concentration $Co = 1.0 \times 10^{-5}$ M by sample chips with an effective surface area of 5 cm^2. Negligible MB degradation is observed for the reference experiments carried out in dark (i.e., without shining of UV light), for samples with SiO_2 film only and sample 2 film without any TiO_2. (b) MB degradation in the presence of 15 nm TiO_2 deposited on sample 1−3; TiO_2/2 nm SiO_2 deposited on sample 1−3. (c) Photocurrent density in pure TiO_2; TiO_2 deposited on sample 2; TiO_2 deposited on sample 2 with SiO_2 interlayer of thickness 2, 5, 10, and 20 nm.

The TiO_2 ALD process performed at a low-temperature of 150 °C will result in an amorphous TiO_2 film.[13,31] It will be beneficial to alter the as-deposited TiO_2 to an anatase phase as that is known to exhibit higher photocatalytic efficiencies.[3,5] Therefore, the ALD TiO_2 are annealed for 2 h at 500 °C to obtain the anatase phase. This is confirmed by both UV -Raman spectroscopy (Figure 4a) and X-ray diffraction (Supporting Information, Figure S1) analysis. The Raman excitation at 325 nm ensured the resonant excitation of TiO_2. It is important to note that, under typical conditions, the UV-Raman detection of the ultrathin TiO_2 (∼15 nm) film is highly improbable because of its low film thickness. In the present case, the underlying Ag nanoparticles provided strong enhancement of the Raman signal, thereby aiding in the detection of the signature Raman spectra of anatase TiO_2. Observed Raman bands at 144 cm^{-1}, 197 cm^{-1}, 396 cm^{-1}, 514 cm^{-1}, and 635 cm^{-1} assigned as the Eg, Eg, B1g, A1g, or B1g, and an overtone Eg, respectively, are consistent with the anatase phase of TiO_2.[32] There are no signature peaks of either the rutile phase (at 610, 446, and 242 cm^{-1}) or any broad peaks (at 600 and 300 cm^{-1}) corresponding to amorphous phase. The inset shows the Raman peak intensity variation of the normalized 144 cm^{-1} band with SiO_2 interlayer thickness. The decrease in Raman intensity of TiO_2 with increase in its distance from the silver nanoparticle layer is in accordance with the distance dependence reported for SERS.[21] However, the decrease of intensity with the thickness of SiO_2 interlayer does not conform to as observed for SERS of molecules such as 4-mercaptopyridine,[33] Rhodamine 6G,[34] and such others dispersed on nanotextured Ag surfaces. These SERS experiments involving molecular and ionic species have been studied extensively.[35−38] In these systems the near electromagnetic (EM)-field enhancement leads to SERS.[37] However, to the best of our knowledge, SERS in Ag/metal oxide structures have been rarely studied.[39] Our system utilizes the SERS of metal oxide TiO_2. In TiO_2, because of its band gap (3.2 eV) close to the Raman excitation wavelength, the far field scattering also plays a major role in the SERS.[40] Because of this fact, the enhancement in the Raman intensity is decreased only by a factor of ∼2 upon having a 10 nm SiO_2 interlayer. Our study shows that for semiconducting systems like TiO_2, with the band gap close to the SERS excitation energy, the far field scattering effect also has a major role to play. Such, variation in enhancement of the intensity, with thickness of SiO_2 interlayer, clearly suggests the different mechanisms responsible for SERS at these length scales and are discussed in a later part of the manuscript. Briefly, at a distance less than 10 nm, the Raman peak intensity enhancement is due to LSPR mediated large near field enhancement, and the far field scattering would still prevail at a distance away.

Optical reflectance spectra is an alternative to the extinction spectra to locate the LSPR in metal nanoparticles on an opaque substrate.[17] Figure 4b shows the reflectance spectra of the samples, with the LSPR being identified as the wavelength of minimal reflectance. The Ag nanoparticle film (Sample 2) exhibits a strong and sharp LSPR at wavelengths around 388 nm that is consistent with other reports.[41,42] For nanoparticles much smaller than the wavelength of light, the EM field is uniform across the particle such that all the conduction electrons move in-phase producing mainly dipole-type oscillations manifested by a single, narrow dip in the LSPR reflectance spectra.[7] Upon having either TiO_2 or TiO_2/SiO_2 film coat over the particles, the LSPR dip is red-shifted. For the 15 nm ultrathin

dx.doi.org/10.1021/cs100117v |ACS Catal. 2011, 1, 300–308

Table 1. Percentage Degradation of Methylene Blue (MB) after 4 h of UV Exposure for All the Samples Studied in This Work

control experiments	% MB degradation after 4 h UV exposure
No UV light exposure (15 nm TiO_2)	3
SiO_2 only	3
Sample 2	8
15 nm TiO_2 amorphous	8
15 nm TiO_2 anatase (pure TiO_2)	44
Pilkington Activ glass slide	49

	% MB degradation after 4 h UV exposure				
		15 nm TiO_2/SiO_2			
	15 nm TiO_2	2 nm	5 nm	10 nm	20 nm
Sample 1	50	88			
Sample 2	55	100	90	82	77
Sample 3	64	66			

TiO_2 a red shift of ~90 nm is observed. A linear relationship between the refractive index of the medium and plasmon resonance is predicted using the Mie theory calculations for spherical silver nanoparticles in a dielectric medium. Malinsky et al have calculated that for a 60 nm diameter particle surrounded by a uniform dielectric medium the peak plasmon resonance wavelength would shift by 2.1 nm per 0.01 index change.[43] Accordingly, a LSPR red-shift of 300 nm can be expected for Ag particles in a bulk TiO_2 (n(400 nm) ~2.5). However, in our case, since the TiO_2 film is only 15 nm thick, a much reduced shift can be expected. With a 2 nm SiO_2 interlayer, a smaller shift of only 40 nm was observed. A more detail examination of the LSPR shift vs SiO_2 film thickness is shown in Figure 4c. It can be seen that an increase in the SiO_2 thickness leads to a much lower red shift and eventually, this is reduced to just 13 nm for the 20 nm SiO_2 interlayer. This trend agrees well with reports in the literature with regards to the influence of coating thickness on the LSPR wavelength of Ag nanoparticles.[23] These have been calculated based on the Mie theory, and also experimentally demonstrated with varying thickness of mica over Ag and also with thickness variation studies using ALD Al_2O_3 as spacer layers.[10,43,23] The SiO_2, with a lower index of 1.54 (at 400 nm), provides a different dielectric environment which offers lower retarding field and also shields from the retarding field from TiO_2. Such a tuning of the LSPR by the SiO_2 is actually beneficial for energy coupling during the TiO_2 plasmonic catalysis since the tuned LSPR wavelength is now closer to the energy band gap of TiO_2.[10] Similar observations have been made by Awazu et al; however, unlike in this work,[10] there are no observed LSPR in their TiO_2/Ag samples. This has been attributed to the oxidation of the Ag nanoparticles that we have prevented presumably because of a different coating condition. This again highlights one of the advantages of using ALD TiO_2 in preserving the stability of the underlying Ag nanoparticles, especially if LSPR properties are desired.

The photocatalysis activities of the samples were investigated by the UV degradation of methylene blue (MB) at room temperature. The degradation of MB on TiO_2 is an oxidative process caused by the holes from the photogenerated e^-/h^+ pair. The remaining electrons are scavenged by dissolved O_2.[44] Figure 5a,b shows the kinetics of photocatalytic degradation of 5 mL MB with a Co concentration of 1.0×10^{-5} M in UV light illumination (with a maxima at 365 nm). Sample chips with an effective surface area of 5 cm^2 were used for the experiments. Appropriate control experiments were performed to ensure negligible MB degradation. The control experiments carried out in the absence of UV illumination (in dark), Ag/SiO_2 film only with no TiO_2 and Ag nanoparticles film (sample 2) in the absence of SiO_2 and TiO_2 coating confirmed negligible MB degradation (Table 1). The 15 nm thin anatase and amorphous TiO_2 mineralizes 44% and 8% of MB, respectively, upon 4 h of UV exposure (Table 1). Although it is often difficult to compare photocatalysis results from several sources as the photoactivity of a sample is highly dependent on exact experimental parameters, we hereby attempt to compare our results with a similar work to highlight the photoactivities of our nanostructured TiO_2 surface. Kaariainen et al. observe a ~58% MB degradation for 15 nm ALD TiO_2 film consisting of a mixture of anatase/rutile TiO_2 phase.[45] This film showed the highest photocatalytic activity, with a decrease for thicker and thinner TiO_2 films. The minor difference in the performance could be due to the differences in the sample preparation procedure. The present study employed post ALD annealing, and the XRD and Raman spectra analysis showed the presence of only anatase TiO_2. Several studies have postulated that the best photocatalytic activity for TiO_2 is reached with an optimum ratio of anatase and rutile phases.[46] The Supporting Information, Table S1 provides detailed information of ALD based TiO_2 photocatalyst reported previously in the literature. The different experimental conditions in many reported literatures prove to be tricky in a quantitative comparison; hence, using an evaluation standard is appropriate. The self-cleaning Pilkington Activ is chosen in this work as an evaluation standard, and it shows a degradation of 49% under the same experimental conditions. Furthermore, the Pilkington Activ glass slides have been well-established for self-cleaning application and are widely available. They are therefore a suitable standard for experimental evaluations as suggested by Mills et al.[47] It is also useful that the Pilkington Activ consists of ~15−20 nm thin layer of nanocrystalline anatase TiO_2 (similar to our thickness of TiO_2) on soda-lime silicate float glass. Having established a good comparison between both our anatase TiO_2 (15 nm) and the Pilkington Activ glass slide, we will now look at the effects of the Ag coated samples. The 15 nm TiO_2/sample 2 shows only a marginal improvement to that of pure TiO_2 (Table 1). However, upon introducing a SiO_2 interlayer, considerable improvement is observed in the photocatalytic performance. The best photodegradation performance is exhibited by the sample with a 2 nm SiO_2 interlayer, showing a 100% MB degradation. The MB degradation kinetics by the plasmonic catalyst having the 2 nm SiO_2 interlayer is ~2.3 times faster than the pure TiO_2. The photocatalytic performance of our samples are comparatively lower than that of plasmonic catalysts reported by Awazu et al.[10] This can be attributed to the ultrathin nature (~15 nm) of the TiO_2 films and also the lower irradiation intensity of 17 $\mu W/cm^2$ employed in our study as compared to 0.5 mW/cm^2 used by Awazu et al. The photocatalytic performance is found to exponentially decrease with an increase in SiO_2 interlayer thickness (Figure 5c). Since ALD is a conformal process, the surface roughness is not expected to be markedly different for different cycles of coatings, and thus surface roughness cannot be a reason for the drop in catalytic performance. Figure 5b shows the photocatalysis performance 15 nm TiO_2 over Samples 1−3,

dx.doi.org/10.1021/cs100117v |ACS Catal. 2011, 1, 300–308

with and without the 2 nm SiO_2 interlayer. The improvement of the catalytic performance is evident for all coverages of Ag. As mentioned above, without any SiO_2 interlayer, the photocatalysis performance is observed to be better with an increase in the underlying Ag concentration. With the introduction of a thin SiO_2 interlayer, we observed that the best photocatalytic performance is actually provided by the Ag coverage of sample 2. This is the sample that consists of Ag nanoparticles in the size range ~60−150 nm. With this information, we systematically discuss and validate the different scenarios that could bring about the observed photocatalytic enhancement in the presence and absence of a SiO_2 interlayer. On the basis of our experimental observations and literature evidence, the photocatalytic enhancement could be best explained by electronic effects in case of TiO_2/Ag films and through plasmonic field effects for TiO_2/SiO_2/Ag architectures.

First, in the absence of a SiO_2 interlayer, the following mechanisms are plausible:

(i) **"Electronic *effect*" due to Fermi level equilibration:** When Ag nanoparticles are in contact with TiO_2, the ensuing Fermi level equilibration results in formation of a Schottky barrier (depletion layer) at the junction.[25] This Schottky barrier enhances charge separation and helps prevent recombination of e^-/h^+ pairs that are generated in the presence of light. Such a charge equilibration results in a higher photocatalytic activity of the TiO_2/Ag nanoparticles film. Increasing the concentration of Ag will therefore increase the photocatalytic kinetics, and this is consistent with our experimental observations as shown in Figure 5b. However, this mechanism can only be dominant for samples without any SiO_2 interlayer, as otherwise the Schottky barrier formation is prohibited. Enhancement of the photocatalytic activities are similarly observed in other independent work when the concentration of Ag in TiO_2 is increased.[4,48,49] However, one important distinction is that unlike our approach, which places the Ag nanoparticles film underneath the TiO_2, a continued increase in the Ag concentration in a composite of Ag-TiO_2 has been shown to lower the photocatalytic activity, and this is not seen in our work. This lowering has been attributed to the UV shielding, passivation of reactive surface sites by Ag, and also reduced crystallinity of TiO_2 in the presence of Ag.[4,48,49] These phenomena are naturally avoided in our work because of the architecture employed.

(ii) **"Surface plasmon mediated electron transfer from Ag to TiO_2"**: One possible avenue of enhanced catalytic activities is due to a LSPR mediated electron transfer. In this phenomenon, the photoexcited electrons in Ag nanoparticles can be transferred to the TiO_2 conduction band, and accompanying that is a simultaneous transfer of compensative electrons from the donor (MB solution) to Ag.[25,50] Since in our architecture, Ag is not in direct contact with the MB solution, this phenomenon cannot be used to explain the enhanced reaction and can be ruled out.

(iii) **"Charge transfer from photoexcited TiO_2 to Ag"**: Transfer of electrons from photoexcited TiO_2 to Ag has been used in some cases to explain for the increase in the photocatalytic efficiency in TiO_2/Ag composites.[51,52] In this instance however, an increase in electronic density at the Ag surface would have caused a blue shift in the LSPR band.[53] Instead, a red shift for both TiO_2/Ag and TiO_2/SiO_2/Ag is observed suggesting the absence of such mechanism.[54] Furthermore, while this can possibly be a contributing factor for the TiO_2/Ag films, such phenomenon should be distinctly absent in the TiO_2/SiO_2/Ag architectures due to the SiO_2 interlayer that physically prevents electrical conduction between TiO_2 and the Ag.

On the basis of arguments in (i)−(iii), the photocatalytic enhancement in the TiO_2/Ag system could be said to be predominantly caused by "*electronic effects*" due to the Fermi level charge equilibration.

The photocurrent measurements shown in Figure 5d provide further insight into charge carrier concentrations in the presence and absence of SiO_2 interlayer. The TiO_2/Sample 2 shows only a marginal increase of ~35 $\mu A/cm^2$ in current density as compared to bare TiO_2 films, and as mentioned, this can be attributed to the electronic effects. However, with the SiO_2 interlayer, we observed a 3-fold increase of current density, representing a high photogenerated carrier concentration. Since such high enhancement is not observed without the SiO_2 interlayer and it is useful to state that the "*electronic effect*" only helps to improve e^-/h^+ pair separation and cannot possibly increase the charge carrier concentration.

With the presence of a SiO_2 interlayer, we will thus consider the following three field effects that are plausible with an LSPR excitation band. In particular, Figures 4b and 4c show that the LSPR reflection minima produce a reduced red shift with the interlayer resulting in an excitation that is closer to the electronic band gap of TiO_2. This indicates that "*LSPR field effects*" could be dominant under these circumstances.[10]

(i) "LSPR Mediated Localized Heating". There can first be localized heating of Ag nanostructures caused by a nonradiative decay of Ag surface plasmons due to electron−phonon interactions.[55] This local heating effect may be expected to cause photocatalysis enhancement by MB degradation. However, it is well-known that the nonradiative decay is only prominent for Ag nanoparticles of sizes of typically below 40 nm.[7] More importantly, if this mechanism were to be dominant, the TiO_2/2 nm SiO_2/sample 1 (with Ag nanoparticles of 10−20 nm) will be expected to show the best photocatalytic performance. This is not observed and instead, the best performance is from samples with Ag particle size of ~60−150 nm (TiO_2/2 nm SiO_2/sample 2). Furthermore, the photocatalysis experiment (Figure 5a) performed directly on Sample 2 in the absence of any TiO_2 shows only 8% degradation of MB, showing that only thermal effects are negligible.[56] Therefore, we rule out the plasmon induced localized heating as a dominant cause for the observed enhancement.

(ii) "LSPR Mediated near Field Enhancement". The LSPR of Ag nanoparticle arrays result in an enhanced spatially confined electrical field close to the particle surface as well as giant field enhancements at the junction of the particles.[57] Energy transfer from Ag to TiO_2 is reported to occur through coupling of the LSPR of Ag with the band gap of TiO_2.[11,58,59] During the energy coupling, the plasmon relaxation occurs via excitation of an e^-/h^+ pair in the semiconductor. This EM field relaxation channel is plausible provided that the plasmon energy is larger than the band gap of TiO_2.[59] If the surrounding medium is an insulator (e.g., SiO_2) with a larger band gap than the plasmon excitation energy, it will remain "inert" to the field. Hence, to utilize the near field effects in photocatalysis applications it is essential to have a maximum overlap of the LSPR band with the electronic bandgap of TiO_2. As shown in Figure 4b−c, without the SiO_2 interlayer, the LSPR is centered at 470 nm while it shifts to 420 nm with a

2 nm thin SiO_2 interlayer. With a further increase in the thickness of the SiO_2 interlayer, the resonance wavelength undergoes a gradual blue shift, and arrives at a wavelength of 390 nm for the sample with a 20 nm thick SiO_2 interlayer. Considering only energy matching, these results suggest that a thicker SiO_2 interlayer would be more beneficial to enhance the overlaps. However, the increase in thicknesss also reduces the penetration depth of the LSPR EM field into the SiO_2 layer.[11] For spherical Ag nanoparticles of size range 50−200 nm, the characteristic decay length is only ∼20 nm.[43] The distance dependence of the decaying EM field close to the particle surface has been studied extensively in the context of SERS. It is known that the intensity of the evanescent field exponentially decreases away from the particle surface. This has also been shown for SiO_2 overlayers coated on Ag substrates.[21] In this context, we have investigated Raman spectral enhancement of TiO_2 signals as a function of SiO_2 interlayer thickness. The Raman spectra (Inset in Figure 4a) shows a 200 times increase in the signal intensity for the sample with 2 nm SiO_2 interlayer, as compared to pure TiO_2. The Raman intensity enhancement would have been much pronounced, with a good match of the excitation wavelength and the LSPR.[60] However, even at an excitation wavelength away from the LSPR we observe the coupling of energy from the Ag Plasmon to the TiO_2. The Plasmon due to collective oscillation of the conduction electrons is present even at these Raman exciation wavelengths, creating an EM field around the particles. However, at the resonant wavelength, this EM field would have maxima. The clear enhancement in the Raman signal intensity due to excitation at 325 nm shows that there exists energy coupling which lead to the observation of all the surface phonon modes for different TiO_2 symmetry. These modes are absent in the case of off-resonant spectra as obtained upon excitation with 517.5 nm. It can be seen, as expected, that the Raman peak intensity decreases with an increase in the SiO_2 interlayer thickness. The peak intensity saturates beyond the SiO_2 interlayer thickness of 10 nm, indicating that the enhancement is essentially a near field effect having little influence at larger separations.[21] We can therefore conclude that a 2−5 nm SiO_2 interlayer between the Ag nanoparticles and the TiO_2 film is actually optimal to achieve maximum EM energy coupling. Furthermore, besides enhancing the creation of e^-/h^+ pairs, the EM field could also prevent their recombination. It has been shown earlier that electric field across TiO_2 promotes the separation of photogenerated e^-/h^+ pairs in electro-assisted photocatalysis.[61] The near field effects are further confirmed from the photocurrent measurements as shown in Figure 5d. The highest photocurrent of 310 $\mu A/cm^2$ is obtained in the sample with a 2 nm SiO_2 interlayer. The photocurrent observed for the 10 and 20 nm SiO_2 interlayer sample is 290 and 250 $\mu A/cm^2$ respectively. This clearly suggests that the near EM field effects are not the only factor in the photocurrent enhancement. Similarly, the photocatalysis kinetics for the 10 and 20 nm SiO_2 interlayer sample (Figure 5a) shows improvement as compared to samples without any SiO_2 interlayer. The Raman spectra (Inset in Figure 4a) for these samples clearly show that the near field effects are minimal above ∼10 nm of SiO_2 thickness inspite of the improved photocatalysis and photocurrent values. This suggests that in addition to the near EM field effects, there is enhancement due to the far field scattering. The 100 times enhancement of the 144 cm^{-1} Raman peak intensity, for the 10 and 20 nm SiO_2 interlayer sample, as compared to pure TiO_2, suggests the presence of these far field scattering effects.

(iii) "LSPR Mediated Rayleigh Scattering Effects". For Ag nanoparticles of dimension >40 nm, the majority of the surface plasmons decay via the radiative Rayleigh scattering process.[62] This mechanism results in the concentration of photons to electronically excite TiO_2 and increase the concentration of e^-/h^+ pairs.[10] This is a phenomenon whereby LSPR mediated focusing of incident light into its local subwavelength neighborhood is often discussed.[10,56] Enhancement in e^-/h^+ pair creation then comes about because of the prolonged optical path of the scattered photons.[11] This can be a reason for the good photocatalytic properties observed for the Ag nanoparticles of 60−150 nm in our work. Furthermore, this can adequately explain the photocurrent and Raman spectra enhancement with even a 20 nm SiO_2 interlayer, because in the absence of any far field effects, this would not have been possible. One additional proof is also present when we examine the sample wherein the TiO_2 film is coated on the textured Ag film (sample 3). Without the SiO_2 interlayer, this is the sample with the best photocatalytic performance. However, this sample upon having a SiO_2 interlayer does not show any signature LSPR, and as expected the highest photocatalytic performance is obtained for sample 2, which showed LSPR and relaxes dominantly by Rayleigh scattering. Nevertheless, for an SiO_2 interlayer of thickness <5 nm, both the near and the far field effects could contribute to e^-/h^+ pair creation in the ultrathin TiO_2, and herein we cannot separate the near- and far-field contributions.

CONCLUSIONS

Plasmonic photocatalyst consisting of conformal TiO_2 film over Ag nanoparticles with a SiO_2 interlayer were prepared using ALD and GD wet chemistry technique. The LSPR mediated far and near field effects in this plasmonic photocatalyst were investigated by precisely tuning the thickness of ALD SiO_2 interlayer. The SiO_2 interlayer due to its lower refractive index facilitates enhanced photocatalysis because of blue shift in the LSPR and efficient energy coupling from Ag nanoparticles to the bandgap of TiO_2 via the near EM field (*near field effect*). In the far field regime, the LSPR mediated radiative Rayleigh scattering process increases the optical path length of the photons in TiO_2 and hence results in an enhanced e^-/h^+ pair creation (*far field effect*). In the absence of the SiO_2 interlayer, the LSPR being away into the visible region, the photocatalysis enhancement in TiO_2 is consequently attributed to the Fermi level equilibration between the Ag and TiO_2 (*electronic effect*). Application of plasmonic field effects into other areas such as in solar cell and water photolysis would benefit from the understanding of the different effects involved, and careful engineering to utilize them at best are essential.

ASSOCIATED CONTENT

Supporting Information. XRD analysis of ALD TiO_2 film and tabulation of literature reports on ALD TiO_2 photocatalysts. This material is available free of charge via the Internet at http://pubs.acs.org.

AUTHOR INFORMATION

Corresponding Author

*Phone: (65) 6874 8124. Fax: (65) 6774 1042. E-mail: kumarm@imre.a-star.edu.sg.

■ ACKNOWLEDGMENT

We gratefully acknowledge Azimuth technologies Pte Ltd, Singapore for providing the ALD machine for carrying out the studies. Financial support from Institute of Materials Research and Engineering under A*STAR Singapore is acknowledged.

■ REFERENCES

(1) Hoffmann, M. R.; Martin, S. T.; Choi, W. Y.; Bahnemann, D. W. *Chem. Rev.* **1995**, *95*, 69.
(2) Mills, A.; LeHunte, S. *J. Photochem. Photobiol. Chem.* **1997**, *108*, 1.
(3) Hashimoto, K.; Irie, H.; Fujishima, A. *Jpn. J. Appl. Phys.* **2005**, *44*, 8269.
(4) Fujishima, A.; Rao, T. N.; Tryk, D. A. *J. Photochem. Photobiol., C* **2000**, *1*, 1.
(5) Linsebigler, A. L.; Lu, G. Q.; Yates, J. T. *Chem. Rev.* **1995**, *95*, 735.
(6) Herrmann, J. M.; Tahiri, H.; Ait-Ichou, Y.; Lassaletta, G.; Gonzalez-Elipe, A. R.; Fernandez, A. *Appl. Catal., B* **1997**, *13*, 219.
(7) Evanoff, D. D.; Chumanov, G. *ChemPhysChem* **2005**, *6*, 1221.
(8) Qamar, M. *Desalination* **2010**, *254*, 108.
(9) Carp, O.; Huisman, C. L.; Reller, A. *Progr. Solid. State. Chem.* **2004**, *32*, 33.
(10) Awazu, K.; Fujimaki, M.; Rockstuhl, C.; Tominaga, J.; Murakami, H.; Ohki, Y.; Yoshida, N.; Watanabe, T. *J. Am. Chem. Soc.* **2008**, *130*, 1676.
(11) Hagglund, C.; Zach, M.; Kasemo, B. *Appl. Phys. Lett.* **2008**, 92.
(12) Peng, K. Q.; Yan, Y. J.; Gao, S. P.; Zhu, J. *Adv. Mater.* **2002**, *14*, 1164.
(13) Kumar, M. K.; Tan, L. K.; Gosvami, N. N.; Gao, H. *J. Phys. Chem. C* **2009**, *113*, 6381.
(14) Klaus, J. W.; Sneh, O.; George, S. M. *Science* **1997**, *278*, 1934.
(15) Oliva, F. Y.; Avalle, L. B.; Santos, E.; Camara, O. R. *J. Photochem. Photobiol. Chem.* **2002**, *146*, 175.
(16) Ku, Y.; Fan, Z. R.; Chou, Y. C.; Wang, W. Y. *J. Electrochem. Soc.* **2010**, *157*, H671.
(17) Hicks, E. M.; Zhang, X. Y.; Zou, S. L.; Lyandres, O.; Spears, K. G.; Schatz, G. C.; Van Duyne, R. P. *J. Phys. Chem. B* **2005**, *109*, 22351.
(18) Gutes, A.; Laboriante, I.; Carraro, C.; Maboudian, R. *J. Phys. Chem. C* **2009**, *113*, 16939.
(19) Bohren, C. F.; Huffman, D. R. *Absorption and Scattering of Light by Small Particles*; Wiley: New York, 1983.
(20) Futamata, M.; Maruyama, Y.; Ishikawa, M. *J. Phys. Chem. B* **2003**, *107*, 7607.
(21) Lacy, W. B.; Williams, J. M.; Wenzler, L. A.; Beebe, T. P.; Harris, J. M. *Anal. Chem.* **1996**, *68*, 1003.
(22) John, J. F.; Mahurin, S.; Dai, S.; Sepaniak, M. J. *J. Raman Spectrosc.* **2010**, *41*, 4.
(23) Whitney, A. V.; Elam, J. W.; Zou, S. L.; Zinovev, A. V.; Stair, P. C.; Schatz, G. C.; Van Duyne, R. P. *J. Phys. Chem. B* **2005**, *109*, 20522.
(24) Magdassi, S.; Grouchko, M.; Berezin, O.; Kamyshny, A. *ACS Nano* **2010**, *4*, 1943.
(25) Yang, L. B.; Jiang, X.; Ruan, W. D.; Yang, J. X.; Zhao, B.; Xu, W. Q.; Lombardi, J. R. *J. Phys. Chem. C* **2009**, *113*, 16226.
(26) Waterhouse, G. I. N.; Bowmaker, G. A.; Metson, J. B. *Appl. Surf. Sci.* **2001**, *183*, 191.
(27) Suzer, S. *Anal. Chem.* **2003**, *75*, 7026.
(28) Havercroft, N. J.; Sherwood, P. M. A. *Surf. Interface Anal.* **2000**, *29*, 232.
(29) Weaver, J. F.; Hoflund, G. B. *J. Phys. Chem.* **1994**, *98*, 8519.
(30) Lim, D. C.; Lopez-Salido, I.; Kim, Y. D. *Appl. Surf. Sci.* **2006**, *253*, 959.
(31) Aarik, J.; Aidla, A.; Mandar, H.; Uustare, T. *Appl. Surf. Sci.* **2001**, *172*, 148.
(32) Zhang, W. F.; He, Y. L.; Zhang, M. S.; Yin, Z.; Chen, Q. *J. Phys. Appl. Phys.* **2000**, *33*, 912.
(33) Wang, Z.; Rothberg, L. J. *Appl. Phys. B: Lasers Opt.* **2006**, *84*, 289.
(34) Dieringer, J. A.; Wustholz, K. L.; Masiello, D. J.; Camden, J. P.; Kleinman, S. L.; Schatz, G. C.; Van Duyne, R. P. *J. Am. Chem. Soc.* **2009**, *131*, 849.
(35) Kneipp, K.; Wang, Y.; Kneipp, H.; Perelman, L. T.; Itzkan, I.; Dasari, R.; Feld, M. S. *Phys. Rev. Lett.* **1997**, *78*, 1667.
(36) Hao, E.; Schatz, G. C. *J. Chem. Phys.* **2004**, *120*, 357.
(37) Willets, K. A.; Van Duyne, R. P. *Annu. Rev. Phys. Chem.* **2007**, *58*, 267.
(38) Haynes, C. L.; Van Duyne, R. P. *J. Phys. Chem. B* **2003**, *107*, 7426.
(39) Wang, R. C.; Gao, Y. S.; Chen, S. J. *Nanotechnology* **2009**, 20.
(40) Wang, C. Y.; Liu, C. Y.; Liu, Y.; Zhang, Z. Y. *Appl. Surf. Sci.* **1999**, *147*, 52.
(41) Arai, T.; Kumar, P. K. R.; Rockstuhl, C.; Awazu, K.; Tominaga, J. *J. Opt. A: Pure Appl. Opt.* **2007**, *9*, 699.
(42) Kelly, K. L.; Coronado, E.; Zhao, L. L.; Schatz, G. C. *J. Phys. Chem. B* **2003**, *107*, 668.
(43) Malinsky, M. D.; Kelly, K. L.; Schatz, G. C.; Van Duyne, R. P. *J. Am. Chem. Soc.* **2001**, *123*, 1471.
(44) Houas, A.; Lachheb, H.; Ksibi, M.; Elaloui, E.; Guillard, C.; Herrmann, J. M. *Appl. Catal., B* **2001**, *31*, 145.
(45) Kaariainen, M. L.; Kaariainen, T. O.; Cameron, D. C. *Thin Solid Films* **2009**, *517*, 6666.
(46) Ohno, T.; Sarukawa, K.; Tokieda, K.; Matsumura, M. *J. Catal.* **2001**, *203*, 82.
(47) Mills, A.; Lepre, A.; Elliott, N.; Bhopal, S.; Parkin, I. P.; O'Neill, S. A. *J. Photochem. Photobiol. Chem.* **2003**, *160*, 213.
(48) Gan, W. Y.; Friedmann, D.; Amal, R.; Zhang, S. Q.; Chiang, K.; Zhao, H. J. *Chem. Eng. J.* **2010**, *158*, 482.
(49) Hu, X. P.; Blackwood, D. J. *J. Electroceram.* **2006**, *16*, 593.
(50) Tian, Y.; Tatsuma, T. *J. Am. Chem. Soc.* **2005**, *127*, 7632.
(51) Hirakawa, T.; Kamat, P. V. *J. Am. Chem. Soc.* **2005**, *127*, 3928.
(52) Subramanian, V.; Wolf, E. E.; Kamat, P. V. *J. Am. Chem. Soc.* **2004**, *126*, 4943.
(53) Henglein, A. *J. Phys. Chem.* **1993**, *97*, 5457.
(54) Liu, Y.; Liu, C. Y.; Zhang, Z.; Wang, C. *Spectrochim. Acta, Part A* **2001**, *57*, 35.
(55) Adleman, J. R.; Boyd, D. A.; Goodwin, D. G.; Psaltis, D. *Nano Lett.* **2009**, *9*, 4417.
(56) Christopher, P.; Ingram, D. B.; Linic, S. *J. Phys. Chem. C* **2010**, *114*, 9173.
(57) Hallermann, F.; Rockstuhl, C.; Fahr, S.; Seifert, G.; Wackerow, S.; Graener, H.; von Plessen, G.; Lederer, F. *Phys. Status Solidi A* **2008**, *205*, 2844.
(58) Zhao, G. L.; Kozuka, H.; Yoko, T. *Sol. Energy Mater. Sol. Cells* **1997**, *46*, 219.
(59) Zhdanov, V. P.; Hagglund, C.; Kasemo, B. *Surf. Sci.* **2005**, *599*, L372.
(60) McFarland, A. D.; Young, M. A.; Dieringer, J. A.; Van Duyne, R. P. *J. Phys. Chem. B* **2005**, *109*, 11279.
(61) Jiang, Z. P.; Wang, H. Y.; Huang, H.; Cao, C. C. *Chemosphere* **2004**, *56*, 503.
(62) Kreibig, U.; Vollmer, M. *Optical Properties of Metal Clusters*; Springer: Berlin, 1995.